Proceedings of the
Annual Stability Conference
Structural Stability Research Council
St. Louis, Missouri, April 16-20, 2013

Axial Capacity of Partially Corroded Steel Bridge Piles

H. Karagah[1], M. Dawood[2]

Abstract

This paper presents the findings of an on-going research study to determine the axial capacity of steel bridge piles with severe, but localized loss of cross-section due to corrosion. A total of 13 I-shaped short steel columns with different degrees of sectional deterioration were tested to determine the remaining axial capacity of the deteriorated members. The deterioration of the cross-section was achieved by reducing the thickness of the webs and flanges near the mid-height of the columns. The reduction in the thickness of the flanges and the webs varied between 0-75% and 0-100%, respectively. In some cases, asymmetrical deterioration of flanges was considered which represents actual deterioration of steel bridge piles that was observed in the field. To simulate conditions of severe corrosion, several of the tested piles also included a reduction of the flange width of up to 50%. A digital image correlation-based non-contact measurement system was used to measure the full-field 3D deformation and strain profiles of the tested specimens. The research findings provide unique input into the effect of localized corrosion on the remaining capacity of individual steel bridge piles.

Introduction

Steel 'H' piles are widely used in various states throughout the US. These members are common in older, 'off-system' bridges which cross small creeks or seasonal streams. Many of these structures have been in service for 50 to 60 years. Extended exposure to repeated wetting and drying commonly results in corrosion of these piles as shown in Fig. 1 Typically, this corrosion is localized within a zone a few feet above and below the water or soil surface as shown in the figure. While the corrosion is typically limited in extent, it can be quite severe resulting in near-total loss of cross-section in some cases. Field observations indicate that corrosion occurs in the form of severe reduction of the thickness of the flanges and web of the H piles. In extreme cases this may result in the formation of small perforations or voids in the web and a reduction of the flange width at some cross-sections along the length of the pile.

This severe degradation has raised concerns among DOT's, bridge engineers and maintenance crews regarding the integrity of the severely deteriorated piles. While deterioration of bridge piles typically triggers maintenance and repair activities, evaluation of the pile condition is often largely qualitative. Further, since corrosion can be quite severe, and highly non-uniform,

[1] Graduate Research Assistant, University of Houston, <hkaragah@central.uh.edu>
[2] Assistant Professor, University of Houston, <mmdawood@central.uh.edu>

prediction of the remaining capacity of the pile can be particularly challenging. One approach is to treat the corrosion as uniform along the length of the pile. Using this approach, one could predict the capacity using well-accepted design principles (AISC 2011; AASHTO 2012) based on the minimum cross-section dimensions of the deteriorated pile recognizing that in some cases, the web or flange may be slender leading to local buckling as the dominant failure mode. On the other hand, if the flange and web are non-slender, the localized corrosion may result in the formation of a plastic hinge at the corroded section resulting in global buckling of the pile at a reduced load.

Figure 1: Deterioration of steel bridge piles

Liu et al. (2005) simulated the corrosion of wide-flange columns by locally grinding and torch-cutting the sections to reduce the flange width. While this approach represented the loss of material induced by corrosion, it did not capture the effect of the increased slenderness of the flanges and the web. Based on their test results, the research team proposed a simplified design approach to predict the capacity of damaged and repaired compression struts.

Test Specimens

An experimental program was conducted in two phases to quantify the loss of capacity in steel 'H' piles with severe but localized corrosion. The test specimens consisted of 32 inch long W4x13 steel columns. This section was chosen because the proportions of the section are similar to those of standard HP sections; namely, the flanges and web are approximately the same thickness and the flange width is equal to the section depth. The length of the columns was selected such that the expected failure mode was inelastic global buckling, similarly to typical steel 'H' piles. A total of 13 short columns were cut from two 20-ft. long W4×13 sections.

In the first phase, a total of seven short columns were tested to evaluate the effect of moderate corrosion on the capacity of steel columns. The test matrix for the first phase is summarized in Table 1. One column was tested as an undamaged control specimen. To simulate the effect of localized corrosion the flanges and webs of the remaining specimens were milled to reduce their thicknesses along a 12 inch long segment at the mid-height of the columns. The flanges and webs were milled in multiple passes at a slow rate to minimize heating and distortion of the remaining material. The thickness of the flanges was reduced by 50% and 75% while the thickness of the web was reduced by 30% and 60%. All of the columns were milled symmetrically and no material was removed from the fillet region at the web-to-flange junction.

Each column was assigned a two-part identifier. The two parts indicate the reduction of the thickness of the flanges and the web respectively.

Table 1: specifications of the first group of the test specimens

reduction of flange thickness [%]	reduction of web thickness [%]	designation	$b_{f,min}$ [in]	$t_{f,min}$ [in]	$t_{w,min}$ [in]	A_{min} [in^2]
0	0	0/0	4.167	0.360	0.303	4.11
	30	0/30	4.170	0.353	0.213	3.74
	60	0/60	4.168	0.357	0.121	3.45
50	0	50/0	4.169	0.155	0.285	2.47
	30	50/30*	4.162	0.183	0.206	2.32
75	0	75/0	4.173	0.072	0.284	1.69
	60	75/60	4.173	0.106	0.106	1.33

* total length of 27 in.

In the second phase, a total of six columns were tested to represent more realistic degradation similar to the corrosion patterns that were observed in the field. Table 2 gives the details of the columns that were tested in the second phase of the experimental program. The simulated corrosion patterns that were used for the second phase of the research are illustrated schematically in Fig. 2. Four of the tested columns included a 2 inch void in the web at the mid height of the column to simulate total through-corrosion of the web. Four of the columns were machined to simulate un-symmetric flange corrosion in which the reduced thickness regions of the two flanges were offset from the mid-height of the column. Three of the columns were machined to simulate severe corrosion resulting in a reduction of the width of the flanges. All of the specimens were machined to simulate reductions of the thicknesses of the flanges and the web of 75% and 60% respectively. Each of the specimens was assigned a five part identifier. The first two parts indicated the reduction of the flange and web thickness respectively. The third part indicated the presence or absence of a void in the web, “V” or “NV” respectively. The fourth part indicated symmetric, “S”, or unsymmetric, “US” corrosion of the flanges. The fifth part of the identifier was used to indicate reduction of the width of the flanges “WR”. The last part of the identifier was excluded for columns in which the flange width was not reduced. For example, the designation “75/60/V/US/WR” indicates a specimen with 75% reduction in the flange thickness, 60% reduction in the web thickness, a 2 inch long void in the web at the mid-height of the column, with unsymmetric reduction of the flanges, and a reduction of the flange width.

Table 2: specifications of the second group of the test specimens

loss of t_f [%]	loss of t_w [%]	Void in web	unsymmetric flange loss	flange width reduction	designation	$b_{f,min}$ [in]	$t_{f,min}$ [in]	$t_{w,min}$ [in]	A_{min} [in^2]
75	60	No	Yes	No	75/60/NV/US	4.174	0.079	0.099	1.01
		No	Yes	Yes	75/60/NV/US/WR	2.086	0.111	0.102	1.04
		Yes	No	No	75/60/V/S	4.173	0.093	0134	0.87
		Yes	No	Yes	75/60/V/S/WR	2.151	0.098	0.119	0.48
		Yes	Yes	No	75/60/V/US	4.184	0.094	0.132	0.87
		Yes	Yes	Yes	75/60/V/US/WR	2.164	0.102	0.131	0.93

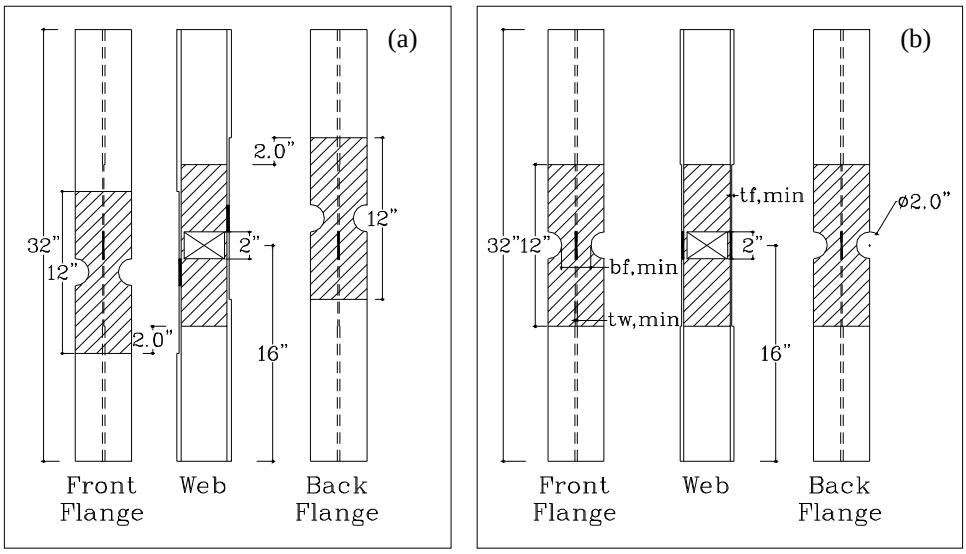

Figure 2: sketch of a asymmetric (a) and symmetric (b) test specimen

To facilitate the use of a digital image correlation (DIC) based measurement system, described below, all of the test columns were painted with a black and white speckle pattern using a matte spray paint.

Test Setup

All the specimens were tested under monotonic uni-axial concentric compression load using a servo-hydraulic Tinius-Olsen universal testing machine with a capacity of 400 kips. The test setup is shown in Fig. 3. The columns were simply supported about their weak axes, while about the strong axis they were fixed-pinned as illustrated in the figure. To minimize unintentional eccentricity, a very thin layer of plaster was cast at both ends of each column before testing. The columns were loaded at a displacement rate of 0.008 in/min up to failure.

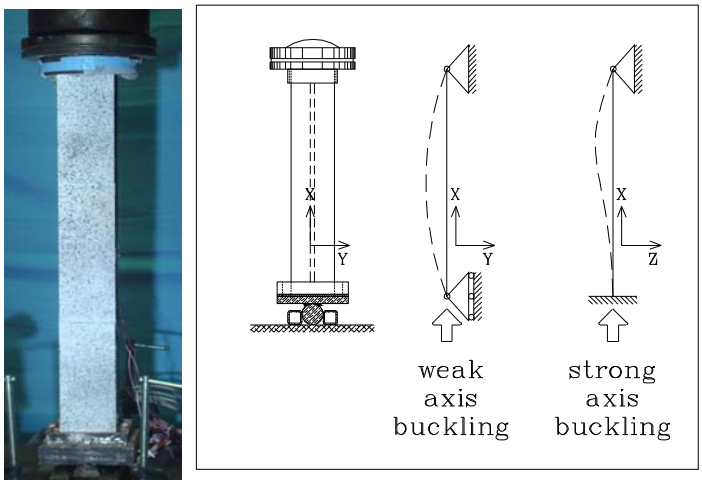

Figure 3: Test setup for concentrically loaded short columns.

Material

A series of tension tests were conducted to determine the mechanical properties of the material used in this study. A total of 6 coupons were tested according to (ASTM A370 2012). Two of the coupons were taken from the web of the section and two coupons were taken from each of the flanges. The coupons were tested using the Tinius-Olsen 400-kip universal testing machine. Axial strains were measured using a 2-inch axial extensometer. The specimens were loaded at displacement rates of 0.025 and 0.200 in/min in the elastic and plastic regions respectively. The mean values of the mechanical properties of the flanges and web are summarized in Table 3.

Table 3: Tension test, results summary

Coupon Designation	Modulus of elasticity	yield strength (0.2% offset)	ultimate strength	strain at ultimate strength	elongation
	[ksi]	[ksi]	[ksi]	[in/in]	[%]
Flange	26925	56.1	69.4	0.13301	29.5
Web	26085	63.7	76.8	0.06962	21.3

Digital Image Correlation System (DIC)

The full-field displacement and strain profiles of the tested columns were measured using a non-contact DIC system known as ARAMIS. The system consists of a pair of 12 Mega Pixel cameras connected to a sensor controller and a high-performance image processing computer. The system is equipped with a special image tracking software. Throughout testing, the cameras capture images of the test specimens at a pre-defined frequency. The image processing software tracks the motion of the speckle pattern on the test specimen. By comparing subsequent sets of images, the software determines the deformation, and consequently the strain, in the specimens between image steps (ARAMIS 2011).

Strains are determined by tracking the movement of user defined clusters of speckles, or facets, on the specimen surface. Fig. 4 shows a set of three square facets that are defined on a random speckle pattern. The facets in the image overlap slightly. Facets are defined by two parameters as illustrate in the figure. The facet size is the number of pixels along each edge of the facets. The facet step is the distance between the center points of adjacent facets, measured in pixels. Fig. 4 shows a grid of three facets with facet size and step of 20 and 16 respectively.

The first image in the measurement sequence represents an undeformed control image under zero load. After assigning a coordinate system to the images and finding the center point corresponding to each facet, the software compares the digital images taken at any load stage with the first image to determine the complete displacement field of the measured surface. Strains are calculated by determining the relative displacements between different sets of facets and dividing by the distance between the facets. The apparent ‘gauge length’ of the strain measurement can be controlled by changing the number of facets used in this calculation, known as the computation size. Fig. 4 illustrates the simplest case with a computation size of 3. The relative displacement between the center points of the outer two facets is used to determine the strain at the center point of the middle facet. Increasing the computation size results in a more averaged strain (larger ‘gauge length’) while decreasing the computation size yields more accurate, but more noisy localized strains (smaller ‘gauge length’).

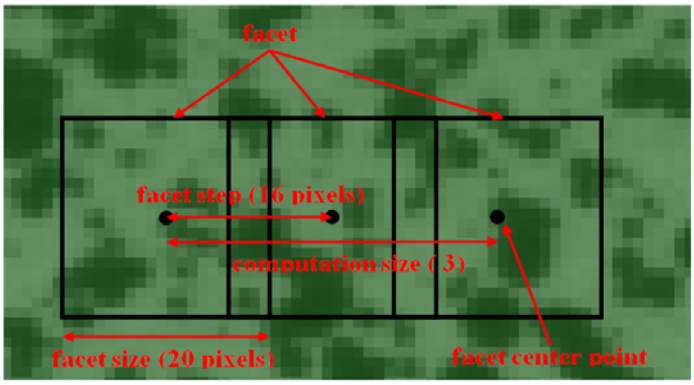

Figure 4: Facet size, facet step, and computation size illustration

To investigate the sensitivity of the strain measurement achieved by the DIC system, a preliminary compression test was designed and performed. A 16-inch long W4×13 stub column, shown in Figure 5, was tested. The bottom end of the specimen during the test rested on the base platen which can be considered as a fixed support while the top edge was bearing against the top cross head of the loading machine which can be simulated as a pinned end. Compression force was applied concentrically using the Tinius-Olsen 400-kip universal testing machine, and deformation of the specimen measured using the DIC system. In addition, four strain gauges were mounted at mid-height on the tips of the flanges for comparison and verification purposes.
To explore the effect of the DIC measurement parameters, i.e. facet size, facet step, and computation size, on the deformation and strain results, a sensitivity analysis was conducted. The parameters are shown in Table 4.

Table 4: Project parameters selected for stub column test

Facet size and facet step [pixel]	15×10	20×16	25×16	30×16
Computation size [points]	3	5	7	19


Figure 5: Stub column test setup

The results of the sensitivity study are shown in Fig. 6. The figures show the measured strain profiles along the outer surface of one flange at a load level of 214 kips. The measured strains from the strain gauges on the tips of the flanges are indicated by the solid diamonds in the figures. The strain distributions along the mid-height of the flange are also shown for different combinations of parameters considered in the study. The figure indicates a slight gradient of strain due to the unintentional eccentricity in the specimen. The effect of the facet size and facet

step is shown in Fig. 6(a). The figure indicates that there was generally a good correlation between the strains measured using the electrical resistance strain gauges and the DIC system. The figure further indicates that changing the facet size and facet step did not have a significant effect on the measured strain profile. Visual inspection indicates that the strain profile with facet size and step of 15×20 exhibited more noise than the strain profiles obtained using other combinations of facet size and step. Among the remaining combinations studied, the strain profile with the facet size and step of 20x16 required the least computational effort. Therefore, it was selected to study the effect of computation size on the measured strain distributions as shown in Fig. 6(b). As can be seen, the various computation sizes provide almost the same strain profile since the local strain gradients were relatively small. Based on the results of the sensitivity study, facet size, facet step, and computation size of 20, 16, and 7 respectively were selected to process the data from the remaining short column tests. All of the columns were painted with a black and white speckle pattern and a pair of cameras was setup to measure strain profiles on the outer face of one of the flanges for the duration of the tests.

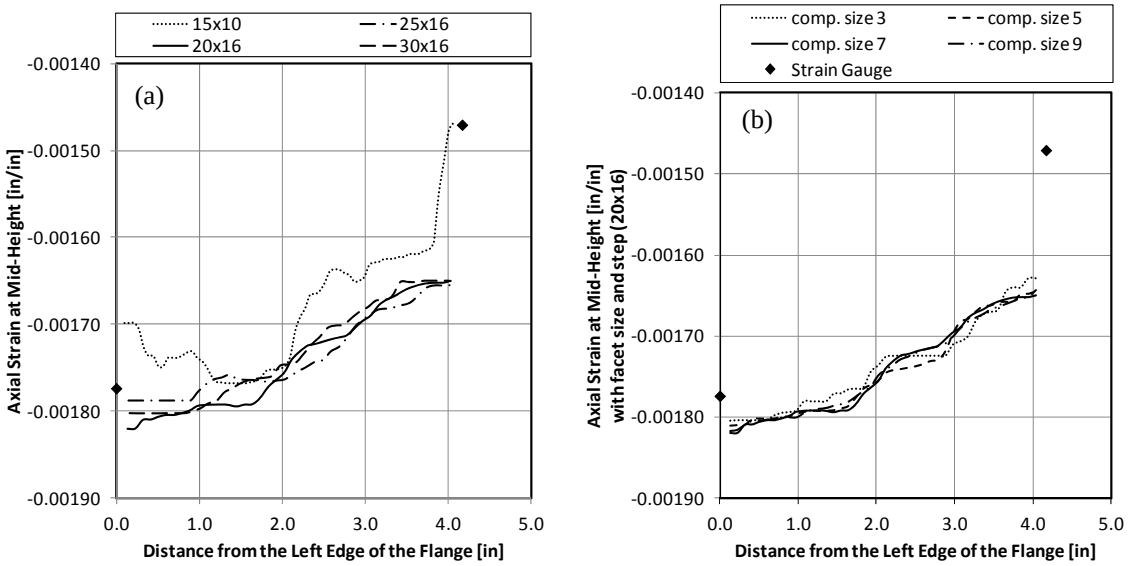

Figure 6: Comparison between the strain gauges and DIC results with (a) different facet sizes and steps, and (b) different computation sizes with the fixed values of facet size and step of 15×10.

Test Results

Table 5 and Table 6 summarize the failure modes and the maximum attained axial compressive load, P_{cr}^{e} of the tested specimens in phase one and phase two respectively. The measured axial strain contours on the outer face of one flange are also given at the peak load for each column. The table also gives the ratio of the measured peak load, P_{cr}^{e} of each specimen to the measured peak load of the un-damaged control specimen, $P_{cr,o}^{e}$ and the ratio of the minimum reduced cross sectional area, A_{min}, to the undamaged gross cross sectional area, A_g. The observed failure modes of the different specimens are also listed in the tables. As expected the failure modes varied from global buckling to flange and web local buckling as the thickness of the cross sectional

elements decreased. Inspections of the measured strain contours also indicates that in many cases, strain concentrations could be identified as localized 'hot spot' strains at the locations where flange local buckling was about to initiate prior to the observation of any visible sign of distress in the specimens.

Comparison and Discussion

Effect of separate web or flange degradation

Comparison of the measured buckling loads for the specimens tested in phase one indicated that corrosion of the flanges had a more significant effect on the overall specimen capacity than corrosion of the webs. The capacity of the cases with only deterioration in the web, "0/30" and "0/60", indicated a reduction of capacity of up to 17% compared to the un-damaged specimen. For the cases with only degradation in the flanges, "50/0" and "75/0", this decrease was up to 57%. It should be noted that the maximum web slenderness, h/tw, for the specimens with 60% reduction of the web thickness was 24.6. This is well below the limit of 32.6 for slender webs as outlined in the AISC and AASHTO specifications (AISC 2011; AASHTO 2012). Thus, none of the specimens had slender webs and therefore, web local buckling was not expected as a dominant failure mode.

Effect of simultaneous web and flange degradation

Although web local buckling was not expected as a failure mode based on the web slenderness, several of the specimens with combined reduction of the flange and the web exhibited a combined failure mode which included both flange and web local buckling. Comparing test columns "0/30" with "50/30" and "0/60" with "75/60" indicates a distinct shift in failure mode. For the specimens with flange and web corrosion, the failure mode was dominated by flange local buckling followed by web local buckling. This was attributed to the fact that buckling of the flanges led to localized distortion of the more slender webs. Inspection of Table 5 generally indicates that reducing the cross-sectional area of the section resulted in a corresponding reduction of capacity. One notable exception is a comparison between test columns "50/0" and "50/30". Although column "50/0" had a greater cross sectional area, column "50/30" demonstrated roughly 10% greater capacity. This can be explained by inspecting the full-field axial strain profile for column "50/0". The strain profile clearly indicates high levels of compressive strains on the left face of the column and much lower strains on the right face indicating weak axis bending of the column. This was attributed to an unintentional eccentricity in the column which is expected to have slightly reduced the measured column capacity.

Effect of the void in the web

Four of the columns tested in phase two included a void in the web. All four of these columns demonstrated the same failure mode; namely buckling of both flanges adjacent to the void in a beam buckling mode rather than a plate buckling mode. All four of these test columns also exhibited comparable failure loads between 36 and 40 kips regardless of the amount and configuration of degradation in other parts of the cross section as shown in Table 6. The results suggest that the loss of support of the flange due to extensive corrosion of the web has a major impact on the overall capacity of the columns.

Table 5: Test Specimens of Phase One, Failure Characteristics and DIC Results

case	0/0	0/30	0/60	50/0	50/30	75/0	75/60
	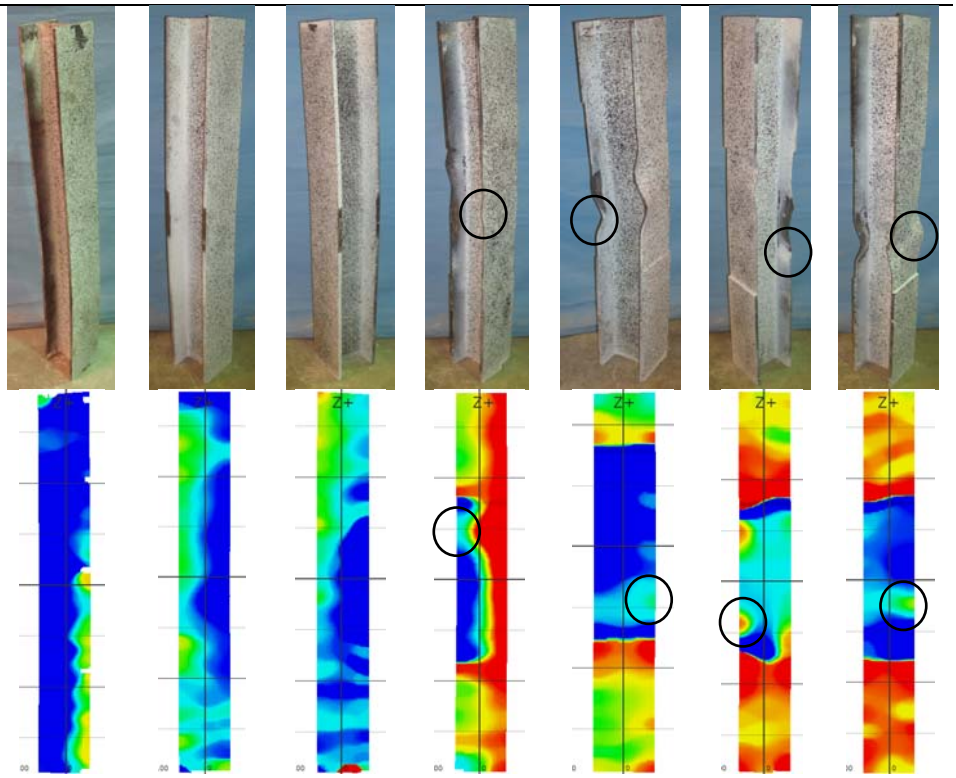						
axial strain at peak load							
Failure mode	GB*	GB	GB	FLB**	FLB /WLB***	FLB	FLB/ WLB
P^e_{cr}[kips]	215	201	178	117	130	92	70
$P^e_{cr}/P^e_{cr,o}$	1.00	0.93	0.83	0.54	0.60	0.43	0.33
$A_{\min}/A_g$	1.00	0.91	0.84	0.60	0.56	0.41	0.32

* Global Buckling
** Flange Local Buckling
*** Web Local Buckling

Effect of unsymmetric degradation

Unsymmetric degradation of the flanges had a minimal effect on the column capacity compared to symmetric degradation. For example, columns "75/60/NV/US" and "75/60" were similar except that the flange degradation of the former was unsymmetrical while the flange degradation of the latter was symmetrical. Comparison of the failure loads indicated a minimal reduction from 70 kips to 57 kips due to the unsymmetry of the flange corrosion. Similarly test columns "75/60/V/S" and "75/60/V/US" failed at equal peak loads as did test columns "75/60/V/S/WR" and "75/60/V/US/WR".

Table 6: test specimens of phase two, failure characteristics and DIC results

case	75/60/ NV/US	75/60/ NV/US/WR	75/60/ V/S	75/60 /V/S/WR	75/60/ V/US	75/60/ V/US/WR
						
axial strain at peak load	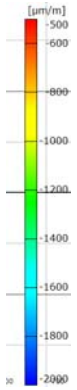	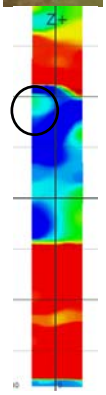	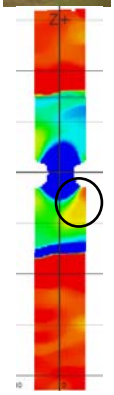	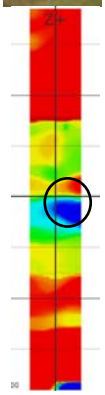	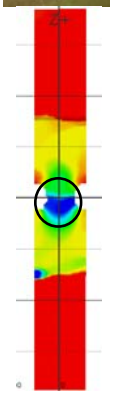	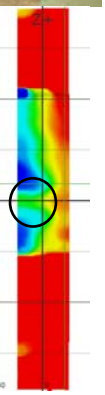
Failure mode	FLB*/ WLB**	FLB/ WLB	FLB	FLB	FLB	FLB
P^{e}_{cr} [kips]	57	70	40	36	40	39
$P^{e}_{cr} / P^{e}_{cr,o}$	0.27	0.33	0.19	0.17	0.19	0.18
$A_{\min} / A_{g}$	0.25	0.25	0.21	0.12	0.21	0.23

* Flange Local Buckling
** Web Local Buckling

Effect of reducing the flange width

The test results indicated that reduction of the flange width had a negligible effect on the column capacity. This can be explained by comparison of the measured strain profiles given in Table 6. The measured strains indicate that size of the buckled region of the flanges was similar to the size of the 2-inch diameter semi-circle that was removed from the edges of the flanges. Since reduction of the flange width reduced the slenderness of the flanges, this deterioration pattern simply shifted the flange local buckling failure mode away from the location of the void as can be seen in Table 6. Comparison of the results in Table 6 further indicates essentially no change in capacity due to the reduction of the flange width.

Effect of reduced cross-section area

Fig.7 summarizes all of the test results from the 13 columns that were tested in phase one and phase two of the experimental program. The figure plots the relationship between the normalized, reduced cross-sectional area, A_{min}/A_g, versus the normalized column capacity, $P_{cr}^e / P_{cr,o}^e$. The solid line represents a prefect correlation while the data points are scattered around the line. Linear regression analysis shows that loss of axial capacity is closely correlated with loss of cross section with an R-squared value of 0.983. This suggests that, for design purposes, the capacity of a corroded pile could possibly be predicted simply by multiplying the design strength of the pile by the ratio of the corroded area of the pile to the gross cross-sectional area of the undamaged pile. This trend is somewhat counter-intuitive since the increase of the slenderness of the individual elements and the formation of a plastic hinge at the corroded section of the pile could reasonably be expected to reduce the critical buckling stress in the pile. This would be expected to have a compounding effect with the reduction of the pile area. This idea is supported by the observed failure modes of the tested columns which showed a shift in failure modes from global to local buckling as flange slenderness increased. However, the data in Fig.7 suggests that the reduction of the cross-sectional area has the predominant effect on the column capacity. One possible factor that may contribute to the observed trend is the localized nature of the simulated corrosion in the relatively short columns that were tested. A different trend may be observed for more slender columns and additional experimental and numerical investigations are being conducted to more fully investigate this behavior.

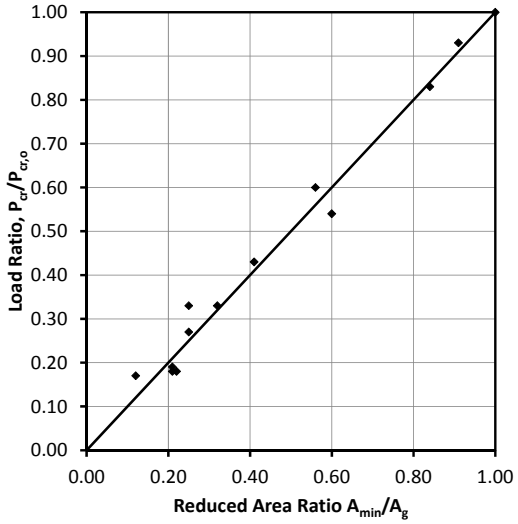

Figure 7: Correlation between loss of cross section and loss of axial capacity

Analysis and Implementation of Existing Design Equations

The provisions of existing design specifications (AISC 2011; AASHTO 2012) were investigated to assess their appropriateness for predicting the remaining capacity of steel compression members with localized corrosion. In order to apply the existing design provisions, the columns were treated as prismatic members with uniform cross-section equal to the reduced cross section in the degraded region. The results of this analysis are presented in Table 7. The slender element correction factors for the flange and the web, Q_s and Q_a, respectively, are given in the table for

reference purposes. Inspection of the table clearly indicates the reduction of the critical buckling stress for corroded sections with slender elements. The table also presents the ratio of the measured peak load to the predicted peak load for all of the tested columns. The table indicates that for cases with moderate levels of simulated corrosion the current design approach predicts the capacity well. However, for cases of extreme corrosion, while being safe, the predicted capacities are overly conservative.

Table 7: Evaluation the axial capacity of the specimens using AISC/AASHTO

designation	loss of cross section [%]	$\left(\frac{b_f}{2t_f}\right)_{\max}$	$\left(\frac{h}{t_w}\right)_{\max}$	Q_s	Q_a	Q_sQ_a	F_{cr}^{a} [ksi]	P_{cr}^{a} [kips]	P_{cr}^{e} [kips]	$\frac{P_{cr}^{e}}{P_{cr}^{a}}$
0/0	0.00	5.80	10.00	1.00	1.00	1.00	53.6	220	215	0.98
0/30	9.00	5.90	14.00	1.00	1.00	1.00	53.6	201	201	1.00
0/60	16.06	5.80	24.60	1.00	1.00	1.00	53.6	185	178	0.96
50/0	39.90	13.40	10.70	0.96	1.00	0.96	51.0	126	117	0.93
50/30	43.55	11.40	14.60	1.00	1.00	1.00	54.1	126	130	1.03
75/0	58.88	29.00	10.70	0.40	1.00	0.40	21.4	36	92	2.56
75/60	67.64	19.70	28.60	0.75	1.00	0.75	40.6	54	70	1.30
75/60/NV/US	75.43	26.40	31.00	0.48	1.00	0.48	25.9	26	57	2.19
75/60/NV/US/WR	74.70	18.70	30.00	0.78	1.00	0.78	41.7	43	70	1.63
75/60/V/S	78.83	22.40	22.80	-	-	-	49.7	43	39	0.91
75/60/V/S/WR	88.32	21.20	25.80	-	-	-	49.6	24	36	1.50
75/60/V/US	78.83	23.30	23.00	-	-	-	49.7	43	40	0.93
75/60/V/US/WR	77.37	20.40	23.20	-	-	-	50.6	47	39	0.83

Fig.8 illustrates the variation of the experimental over predicted axial capacity ratio versus the percentage of the cross sectional area loss. Generally, it can be concluded that if the loss of cross section is less than 50% the design approach in the current specifications, which requires the assumption of uniform corrosion along the entire length of the member, predicts the reduced capacity of the deteriorated columns relatively accurately. Similarly, in the case of a void or 100% loss of the web at a localized cross-section, the capacity of the deteriorated column can be calculated by treating the two remaining portions of the flanges at the corroded cross-section as short, prismatic columns with fixed ends. In this case, the existing design approach predicts the capacity well. However, for other cases when the loss of cross section exceeds 50% the existing design models may be overly conservative.

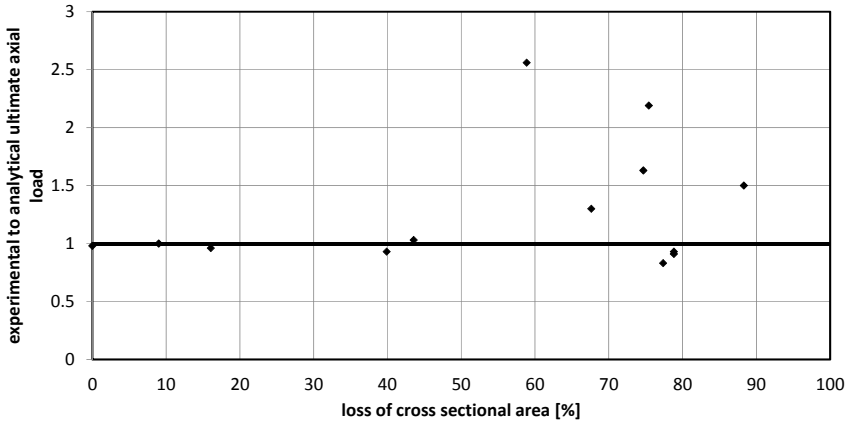

Figure 8: Variation of experimental to analytical capacity ratio by decreasing the cross section

Although the existing design equations were found to be quite conservative for cases of extreme corrosion, they were employed to investigate the effect of flange and web corrosion on overall column capacity. The capacity of the tested W4x13 section was predicted for different amounts of flange and web corrosion range from no corrosion to total corrosion of the flanges or web as illustrated in Fig.9. Since the majority of the out of plane buckling stiffness of the section comes from the flange stiffness, the modulus of elasticity and yield strength of the flange obtained from steel coupon test were used for this evaluation. The dotted line in Fig.9 shows the case with a 2-inch void in the web and treating the two flanges as two short, fixed ends columns which buckle in a beam bending mode. The measured capacities of the tested beams are also plotted for comparison purposes.

Inspection of the figure indicates that the axial capacity is much more sensitive to flange corrosion than to the web corrosion. As illustrated in Fig.9, the experimental data points are very close to the analytical curve for the cases with low percentage of flange degradation, however, deviation increases by increasing the level of the flange thickness reduction.

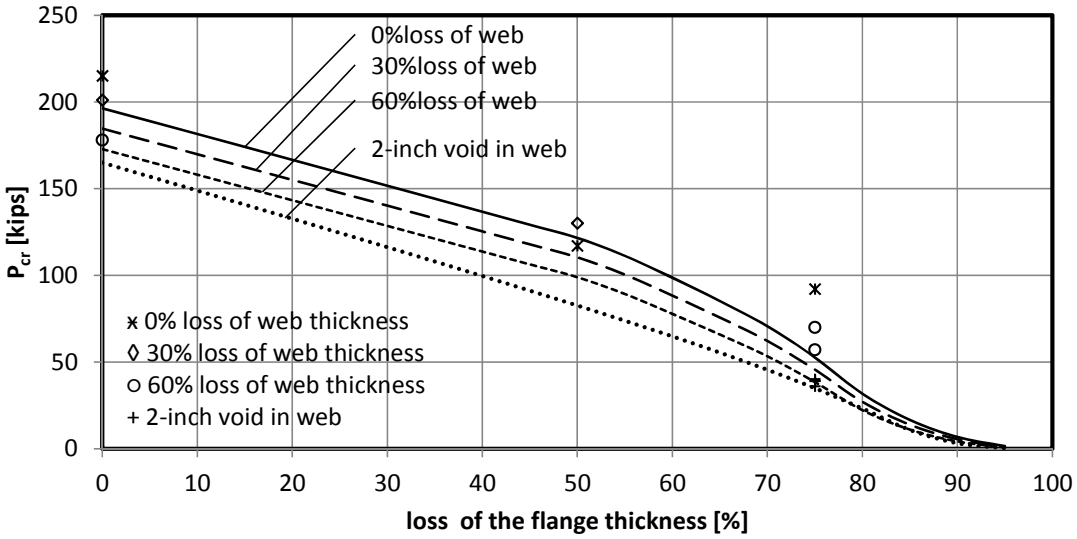

Figure 9: Variation of maximum axial strength of W4×13 and comparison with experimental results

The analytical approach was subsequently extended to investigate the behavior of full-scale steel 'H' piles. A 15 foot long, simply supported HP12×53 pile was selected for the parametric investigation. This pile geometry was selected in consultation with state bridge engineers and is representative of the geometry and assumptions used in the design of these types of piles. The predicted capacities of the corroded piles using the existing design codes and the associated simplifying assumptions are given in Fig.10. The figure emphasizes that the behavior of the piles is dominated by the flange corrosion rather than by the web corrosion. Such design charts could be easily used in the field to conservatively provide a quick estimate of the capacity of a corroded pile based on the known dimensions of the corroded and uncorroded sections of the pile.

The effect of column slenderness on the capacity of the corroded piles was evaluated by varying the length of the HP12×53 piles from 10 ft. to 20 ft as illustrated in Fig.10(b). In this illustration, since web corrosion was found to play a secondary role, corrosion of the web was assumed to be constant and equal to 30%. The length of the piles had a significant effect on the pile capacity

for piles with minor loss of section in the range where global buckling dominated the failure. However, as the degree of corrosion increased, and as flange buckling began to dominate the failure, the length of the piles had little effect on the capacity as one might expect.

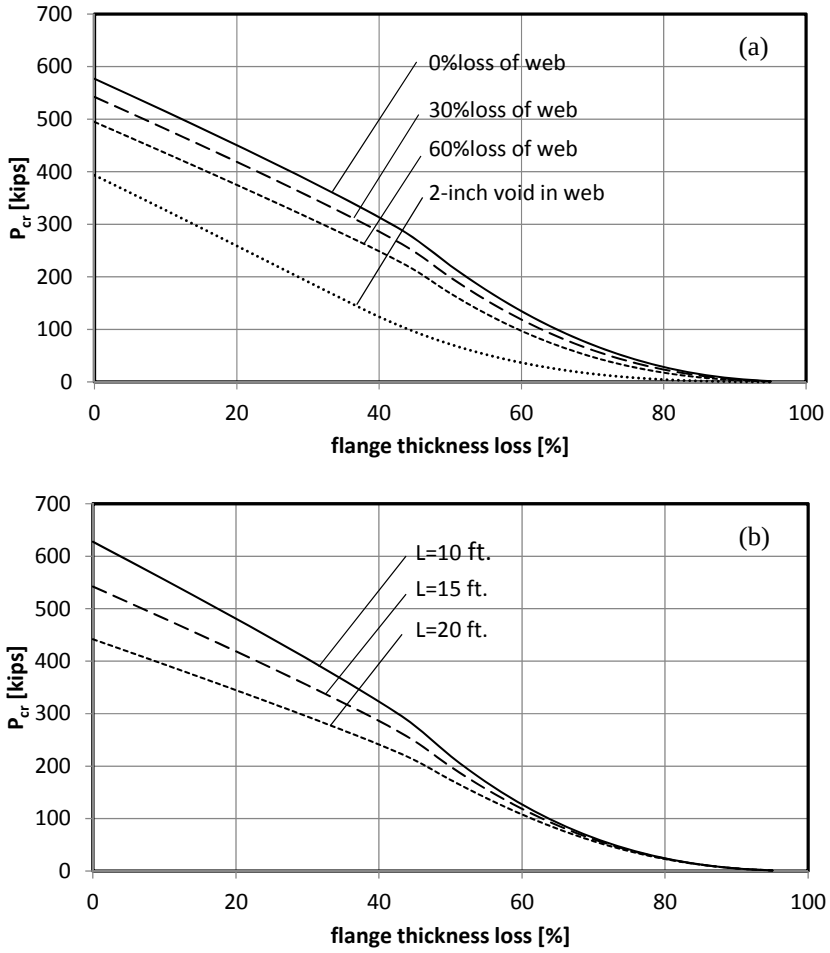

Figure 10: (a) Effect of web and flange corrosion on axial capacity of HP12x53 piles with kL=15 ft. (b) Effect of effective length on axial capacity of deteriorated HP12x53 section with 30% reduction of the web thickness

Summary and Conclusions

A series of artificially degraded short columns were tested under uniaxial monotonic compression to investigate the effect severe but localized damage due to corrosion in steel bridge piles. A digital image correlation (DIC) system was utilized to measure the displacement and deformation. Using the design provisions in existing specifications the axial capacity of the tested specimens was predicted and compared with the experimental results. The analysis was extended to conduct a parametric study of full-scale HP12×53 bridge piles. The following conclusion can be drawn of this study:

- Flange corrosion had a greater effect on the capacity of the piles than web corrosion. In addition, for some cases with slender flanges and moderately corroded webs, distortion in the web was observed although the web was not considered a slender element.

- Unsymmetric degradation of the flanges did not result in a significant drop of the observed capacity of the columns as compared to piles with symmetric flange corrosion. Similarly localized reduction of the flange width did not have a significant effect on the pile capacity.
- In the case of severe corrosion with a void in the web, the loss of capacity was more than 80%. The failure mode for these columns was primarily lateral buckling of the flanges which acted as fixed ends columns with an effective length equal to the length of the void in the web.
- The reduced capacity of the tested short columns was proportional to the cross-sectional area of the columns. This suggests that the reduction of the critical buckling stress due to the increase of the slenderness of the columns did not play a significant role in the reduction of their capacities. Additional experimental and numerical studies are ongoing to evaluate this correlation for piles with different slendernesses and cross-sectional geometries.
- Existing provisions in current design specifications were used to predict the capacity of the tested columns by assuming uniform corrosion along the entire length of the columns. The current provisions accurately predicted the capacity of columns for which the loss of cross section was less than 50%. For columns with severe corrosion the existing design provisions were safe but overly conservative.
- Parametric study was conducted on two I-shaped sections, W4×13 and HP12×53. This study confirmed that the axial capacity is more sensitive to the flange degradation rather than web deterioration. It also showed that the axial strength of the compressive members with less degradation in the flange thickness is more sensitive to the length of the column compared to ones with higher level of the flange deterioration. The analysis was used to illustrate the development of design curves that could be used by maintenance crews during field inspections to quickly determine the remaining capacity of deteriorated piles based on the measured dimensions of the corroded and uncorroded sections of the pile.
- The DIC system indicated the formation of localized strain concentrations at critical locations where flange buckling was imminent. These strain concentrations could be identified well before any visible sign of buckling was observed.

Acknowledgments

The authors would like to acknowledge the financial support provided through TxDOT project 0-6731 ‘Repair Systems for Deteriorated Bridge Piles’. The authors additionally acknowledge the contributions of Mr. Leon Flournoy and Mr. Dingyi Yang who provided valuable insight into the ‘standard practice’ in bridge design. The assistance of Ms. Cheng Shi, Mr Mossab El-Tahan, Mr. William Sagastizado and Mr. Jeffery Miller during the experimental portion of the study is gratefully acknowledged.

References

AASHTO LRFD Bridge, Design Specifications. American Association of State Highway and Transportation Officials (AASHTO), 2012.

ARAMIS User Manual - Software. Braunschweig, Germany: GOM mbH, Optical Measuring Techniques, 2011.

ASTM Standard A370-12a, "Standard Test Methods and Definitions for Mechanical Testing of Steel Products". West Conshohocken, PA: ASTM International, 2012.

Liu, Xiangdong, Antonio Nanni, and Pedro F. Silva. "Rehabilitation of Compression Steel Members Using FRP Pipes Filled with Non-expansive and Expansive Light-weight Concrete." *Advances in Structural Engineering* 8, no. 2 (2005): 129-142.

Steel Construction Manual. 14th. American Institution of Steel Construction (AISC), 2011.